



# North Pacific storm track response to the mesoscale SST in a global high-resolution atmospheric model

Chao Zhang<sup>1</sup> · Hailong Liu<sup>2,3</sup> · Jinbo Xie<sup>2,3</sup> · Pengfei Lin<sup>2,3</sup> · Chongyin Li<sup>1,2</sup> · Qian Yang<sup>2,3</sup> · Jie Song<sup>2,3</sup>

Received: 3 July 2019 / Accepted: 21 June 2020 / Published online: 25 June 2020  
© Springer-Verlag GmbH Germany, part of Springer Nature 2020

## Abstract

The response of the North Pacific storm track to the mesoscale sea surface temperature (SST) in winter is investigated via a global high-resolution atmospheric model. A simulation forced by eddy-resolving SST is compared with a simulation in which the mesoscale SST is filtered out. The results show that removing the mesoscale SST could greatly influence the storm track in the free atmosphere, with a significant decrease of approximately 20% in the local region and a southward shift downstream over the eastern North Pacific. Compared with those in previous studies, the responses of the storm track seem to be independent from models. The underlying mechanism is that changes in the boundary layer induced by mesoscale SST lead to convergence at the surface through pressure adjustment, forcing a secondary circulation along Kuroshio and Oyashio confluence region (KOCR). Then the winter mean vertical eddy fluxes are greatly suppressed over KOCR after removing the mesoscale SST, transporting less heat and moisture into the free atmosphere. Furthermore, the response of baroclinicity and baroclinic energy conversion was investigated, which bears much resemblance with the changes of storm track, indicating the important role on the response of storm track to mesoscale SST.

**Keywords** Storm track · Mesoscale SST · Air–sea interaction · CAM4

## 1 Introduction

Storm tracks, known as the particular regions where activities of synoptic-scale atmospheric eddies are vigorous, play a critical role in transporting heat and moisture between subtropics and the mid-latitudes regions, and thus shaping the weather and climate of the Earth (Hoskins and Valdes 1990; Chang et al. 2002). In recent decades, numerous studies have investigated the mechanisms of storm tracks (Lau and Nath 1991; Straus and Shukla 1997; Sampe et al. 2010).

The intensity and location of storm tracks can be influenced not only by internal atmospheric processes such as the variations of jet streams (Lee and Kim 2003), low frequency events (Zhang and Held 1999), but also by external oceanic processes such as El Niño and the Southern Oscillation (ENSO) and Pacific Decadal Oscillation (PDO), the ocean basin scale sea surface temperature (SST) anomalous patterns (Straus and Shukla 1997; Chu et al. 2020).

Recently, the impacts of mesoscale oceanic eddies and fronts on the storm track have received considerable attention due to the application of high-resolution observation data and model results. In comparison with those processes at large scales which show the ocean is being forced by the atmosphere, the air–sea interactions at mesoscales exhibits a different result. Chelton et al. (2004) revealed a positive correlation between mesoscale sea surface temperature (SST) and surface wind speed, which suggests that the wind speed will be accelerated (decelerated) over warm (cold) eddies. This conclusion has also been confirmed in results of high-resolution models by Bryan et al. (2010).

Furthermore, these mesoscale structures have been reported that they have great impacts on the boundary layer and the free atmosphere (Minobe et al. 2008; Frenger et al. 2013; Chen

✉ Hailong Liu  
lhl@lasg.iap.ac.cn

✉ Chongyin Li  
lcy@lasg.iap.ac.cn

<sup>1</sup> College of Meteorology and Oceanography, National University of Defense Technology, Nanjing 211101, China

<sup>2</sup> State Key Laboratory of Numerical Modeling for Atmospheric Sciences and Geophysical Fluid Dynamics, Institute of Atmospheric Physics, Chinese Academy of Sciences, Beijing 100029, China

<sup>3</sup> College of Earth and Planetary Sciences, University of Chinese Academy of Sciences, Beijing 100049, China

et al. 2017). Ma et al. (2015) examined the remote influences of mesoscale eddies on the North Pacific storm track using a high-resolution regional model. Their results showed that by removing the mesoscale SST, the storm track shifts southward in the eastern North Pacific, accompanied by rainfall variability along North America. They further highlighted the influence of mesoscale SST on the intensity of the storm track (Ma et al. 2017). The significant decrease in the intensity of the local storm track due to the smooth of the mesoscale SST could only be identified in the high-resolution model, while no response to the smooth of the mesoscale SST was found in the low-resolution simulations. More recently, Foussard et al. (2018) explored the response of the tropospheric storm track to mesoscale oceanic eddies in an idealized atmosphere model. Their results showed a robust northward shift in the storm track when the ocean is filled with mesoscale eddies.

However, there are still several uncertainties. For instance, previous studies, such as Ma et al. (2017) and Foussard et al. (2018), are based on a regional model. Therefore, will the results from a global model be as same as those from a regional model? Furthermore, do the results from different models also reproduce the local decrease and meridional shift in the storm track? In this paper, we will investigate the influence of mesoscale SST on the North Pacific storm track using a global high-resolution atmospheric model, the Community Atmosphere Model (CAM).

In addition, the imprints of mesoscale oceanic eddies on the atmospheric boundary layer are straightforward and well documented (Small et al. 2008), while the process and details of their influence on the storm track remain unclear. Ma et al. (2017) mainly focused on the response of the storm track by carrying out diagnostic analyses on the free atmosphere, while the process connecting the boundary layer and free atmosphere has not been adequately investigated. To this end, we will examine the response of the boundary layer to the mesoscale SST, as well as the dynamics that contribute to the variation in the storm track.

In the present study, our main objective is to confirm the response of the storm track to the mesoscale SST using a global atmospheric model and to examine the underlying mechanisms. The paper is organized as follows. Section 2 presents the model experiments and analysis methods. The model evaluation is shown in Sect. 3. Section 4 analyses the response of the storm track. The dynamics are examined in Sect. 5. Finally, the conclusions and discussion are presented in Sect. 6.

## 2 Model and methods

Feliks et al. (2004) and Minobe et al. (2008) have suggested that the impact on the atmosphere by small-scale SST anomalies can be captured only when the resolution

of the atmospheric model is less than 50 km. In this study, we employ a global high-resolution atmospheric model, Community Atmosphere Model version 4 (CAM4; Neale et al. 2013), which uses the Finite Volume dynamical core with approximately 25 km horizontal resolution and 26 vertical levels. To spin up, we firstly run the model for 5 years with the “present-day” greenhouse gas conditions. It uses the default monthly climatological SST as the surface boundary condition. The last day’s output of the spin-up integration was applied as the initial value field of following experiments. Then, the SST boundary conditions of these experiments are taken from a six-year daily mean output from a high-resolution coupled model with a horizontal resolution of  $0.1^\circ \times 0.1^\circ$  (Lin et al. 2019). Compared with the observations, the oceanic eddies are well resolved at this resolution, and the ocean mesoscale structure-induced air–sea interaction is effectively reproduced.

To detect the influence of mesoscale SST, two simulations are conducted. One is forced with the original high-resolution SST field, which is referred to as the control run (CTRL), while the other is forced with a low-pass spatial filtered SST field and referred to as the mesoscale-SST-filtered run (MSFR). To obtain the low-pass filtered SST field in MSFR, a  $5^\circ \times 5^\circ$  spatial boxcar filter used by Small et al. (2019) and Zhang et al. (2019) is applied on the daily SST. The colors in Fig. 1a and contours in Fig. 1b show the winter mean SST in the two simulations, respectively. Compared with CTRL, the SST in MSFR is smoother, and their differences (MSFR minus CTRL) show that most of the SST differences are confined within the Kuroshio and Oyashio confluence region (KOCR;  $33^\circ\text{N}$ – $45^\circ\text{N}$ ,  $145^\circ\text{E}$ – $180^\circ\text{E}$ ). Through the boxcar filter, mesoscale SSTs with wavelengths less than 500 km are significantly removed (Fig. 1d). Both of the CTRL and MSFR simulations were integrated for 6 years.

In fact, sharp SST fronts exist in the KOCR, which is also known as the subarctic front zone (Taguchi et al. 2009). A number of studies have revealed that the meridional shift in oceanic fronts could have a great impact on the atmospheric circulation (Frankignoul et al. 2011), modulating the location and intensity of the storm track (Kuwano-Yoshida and Minobe 2017; Yao et al. 2018). Figure 1c illustrates the zonal mean of the meridional SST gradient between  $145^\circ\text{E}$  and  $180^\circ$ . The axes of the climatological SST gradient in CTRL and MSFR are both located at approximately  $41^\circ\text{N}$ , showing no shift in oceanic front. The maxima are  $1.68^\circ\text{C}/100\text{ km}$  in CTRL and  $1.52^\circ\text{C}/100\text{ km}$  in MSFR. Furthermore, the magnitude of oceanic front represented by the area-averaged meridional SST gradient within KOCR decreased only 4% in MSFR compared to CTRL, which indicates that the influence of oceanic fronts within KOCR may be not dominant in the filtered SST. But the influence of the meridional mesoscale

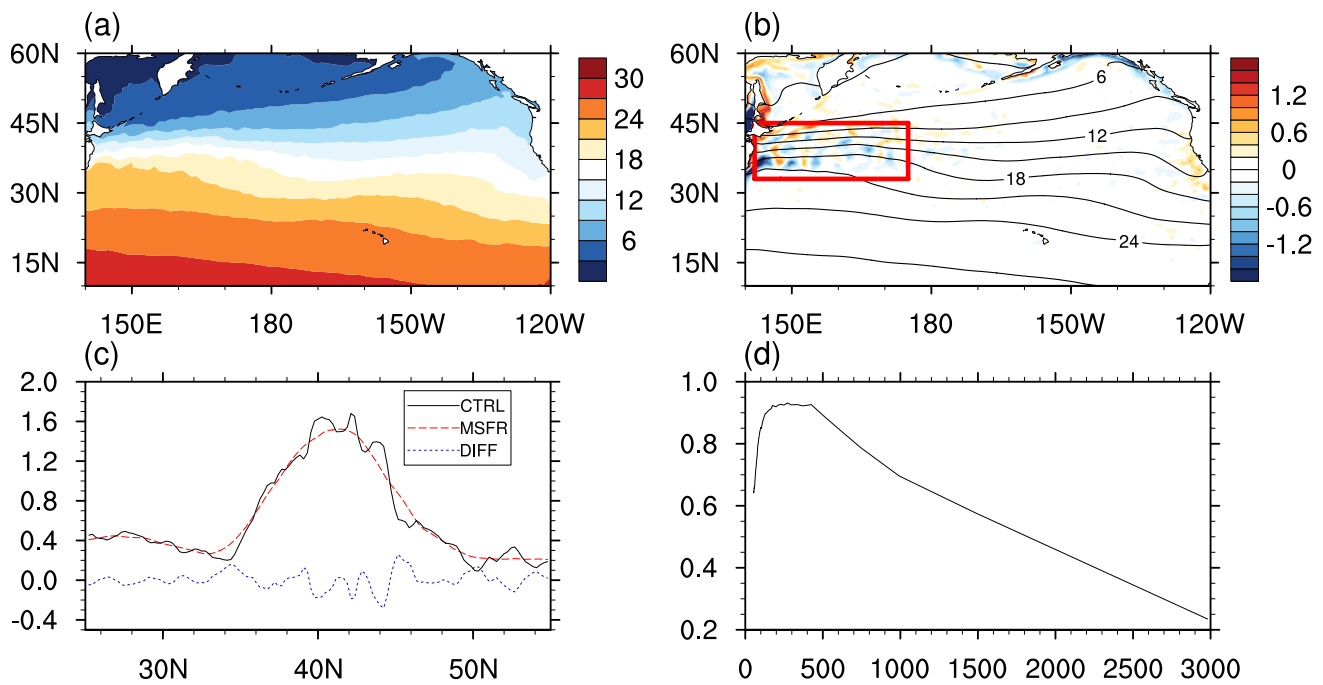


**Fig. 1** Winter mean climatology of SST (units: °C) in **a** CTRL and **b** MSFR (contours; CI = 3 °C). The colors represent the differences (units: °C) in the winter mean SST between CTRL and MSFR (MSFR minus CTRL). **c** The zonal mean (145°E–180°E) of the meridional gradient of SST (units: °C per 100 km) in CTRL (black) and

MSFR (red). The blue line represents the difference between CTRL and MSFR. **d** The ratio of high-pass filtered SST power spectra to original SST power spectra in CTRL in the domain (35°N–45°N, 145°E–180°E). The x-axis denotes wavelength (km)

signal of SST front is worth to investigate in the future by using more sophisticated filter.

Following previous studies (Trenberth 1991; Hoskins and Hodges 2002; Yao et al. 2017), the storm track in this paper is mainly measured by eddy components of meridional heat flux ( $v'T'$ ), specific humidity flux ( $v'q'$ ) and meridional wind variance ( $v'v'$ ), while the prime indicates a 2–8 day Lanczos bandpass filter. In addition, this paper focuses on the boreal wintertime, which is defined as October to February (ONDJF).

As indicated by Alexander et al. (2002) and Seager et al. (2010), the atmospheric circulation in the North Pacific may be strongly influenced by El Niño–Southern Oscillation (ENSO) teleconnections. In this paper, the ENSO signal, which is estimated by the first principal component (PC1) of monthly SST anomalies in the tropical Pacific between 12.5°N and 12.5°S, has also been linearly removed. Considering that the atmospheric response takes a few months to fully develop, a 2-month lagged regression is applied following Frankignoul et al. (2011), Gan and Wu (2013), and Révelard et al. (2016). The linear trend of the storm track is also removed.

In addition, the statistical significance of the differences between the CTRL and MSFR simulations are estimated with a nonparametric approach by bootstrapping. According to the bootstrap method, samples are obtained randomly

from the winter months in CTRL and MSFR. Then, the difference is calculated for every bootstrap sample. To estimate the confidence interval, the procedures mentioned above are repeated 1000 times to assess the distribution of the differences.

### 3 Model evaluation

Before comparing the CTRL and MSFR simulations, we first compare the climatology of the model to the European Centre for Medium-Range Weather Forecasts interim reanalysis (ERA-Interim) data (Dee et al. 2011). As indicated by previous studies (Masunaga et al. 2015, 2016; Booth et al. 2017; Parfitt et al. 2017), the resolution of SST in ERA-Interim has been improved twice from  $1.0^\circ \times 1.0^\circ$  before December 2001 to  $0.05^\circ \times 0.05^\circ$  since February 2009, leading to some artificial impacts on the atmosphere. For this reason, only the period from 2009 to 2017 is used, which covers 8 winters in total.

#### 3.1 Zonal wind and storm track

Figure 2a shows the winter climatological zonal-mean zonal wind ( $[\bar{u}]$ ) between 120°E and 120°W in ERA-Interim and CTRL in latitude–pressure cross sections, where  $[\ ]$  stands

for zonal average, while the notation  $\bar{\phantom{x}}$  means time average. In agreement with ERA-Interim, the simulated zonal wind in CTRL shows a maximum intensity at 200 hPa. From the bottom to the top of the troposphere, the observed  $[\bar{u}]$  is reasonably represented in the model, except that the upper-level zonal wind shifts slightly northward. Figure 2b, c shows the winter climatological zonal averaged storm track, represented by meridional eddy heat flux ( $[v'T']$ ) and meridional eddy wind variance ( $[v'v']$ ), respectively. In both ERA-Interim and CTRL, there are two maximum centers for  $[v'T']$ . One is at 850 hPa above the KOCR, while the other is located at 200 hPa. Compared with the storm track in ERA-Interim, the simulated storm track also shows a slight northward shift. In contrast to Fig. 2b, the location of  $[v'v']$  is well represented in CTRL. However, the amplitude is slightly stronger in CTRL than in ERA-Interim.

### 3.2 Response of surface atmosphere to the mesoscale SST

In this manuscript, we use a  $5^\circ \times 5^\circ$  spatial boxcar filter to separate the mesoscale signals. Firstly, we applied the  $5^\circ \times 5^\circ$  spatial boxcar filter on the original field ( $X$ ) and then the smoothed field ( $\langle X \rangle$ ) is obtained. Subsequently, the mesoscale signal ( $X^*$ ) is derived by subtracting the smoothed field from original one. This procedure is denoted as high-pass boxcar filter and can be expressed as  $X^* = X - \langle X \rangle$ , where  $\langle \phantom{x} \rangle$  denotes the low-pass boxcar filter.

Bishop et al. (2017) has revealed that the air–sea interaction depends on the scale and they pointed out that the oceanic forcing is dominant at the mesoscale in the western boundary currents. To estimate the strength of oceanic forcing on the atmosphere in CAM4, the linear regression coefficients between mesoscale SST and surface wind speed, as well as the turbulent heat flux, are calculated. Here, the surface wind is derived from the bottom model

level. Figure 3a shows the winter mean surface wind speed overlaid on mesoscale SST in CTRL. There is a clear coherence between mesoscale SST and surface wind speed, with the pattern correlation coefficient up to 0.57 in KOCR. The coupling strength is  $0.21 \text{ m s}^{-1} \text{ }^\circ\text{C}^{-1}$  (Fig. 3b), which is in good agreement with Piazza et al. (2016). Their observations also showed that the regression coefficient is  $0.29 \text{ m s}^{-1} \text{ }^\circ\text{C}^{-1}$  in the Gulf Stream (see their Fig. 4d). Similarly, the winter mean mesoscale turbulent heat flux (THF), which is the sum of latent heat flux and sensible heat flux, is shown in Fig. 3c. Here, the release of flux upward is defined as positive. There is a highly positive correlation between mesoscale SST and THF, with the coefficient reaching 0.89 in KOCR. As shown, more heat is released out of the ocean into the atmosphere over warm eddies. The regression coefficient between mesoscale SST and THF is  $45.68 \text{ W }^\circ\text{C}^{-1}$ , which is consistent with previous studies ( $\sim 46 \text{ W }^\circ\text{C}^{-1}$ ; Ma et al. 2017). The uncertainty of the regression coefficient is  $0.49 \text{ W }^\circ\text{C}^{-1}$  for mesoscale THF and only  $0.008 \text{ m s}^{-1} \text{ }^\circ\text{C}^{-1}$  for mesoscale wind speed, respectively.

Overall, the high-resolution CAM4 has a reasonable representation of the jet stream and storm track. CAM4 also shows high fidelity in simulating the responses of surface turbulent flux and surface wind to the mesoscale SST anomalies in KOCR, which gives us confidence to investigate the response of the storm track to the mesoscale SST.

### 4 Storm track response to mesoscale SSTs

To investigate the response to mesoscale SST anomalies, we show the differences in the storm track during winter time over the North Pacific in Fig. 4. For clarity, the difference is defined as MSFR minus CTRL. In addition, the ENSO influence on storm track is linearly removed before calculating the differences.

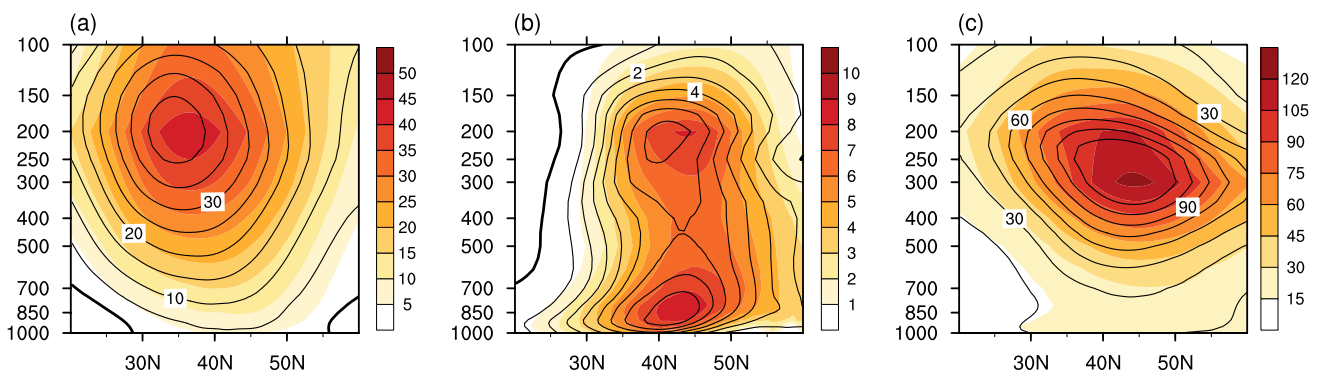


**Fig. 2** Zonal and time averaged **a** zonal wind ( $\text{m s}^{-1}$ ), **b** meridional eddy heat flux ( $v'T'$ ;  $\text{m K s}^{-1}$ ) and **c** meridional eddy wind variance ( $v'v'$ ;  $\text{m}^2 \text{ s}^{-2}$ ) in CTRL (shaded) and ERA-Interim (contours). The contour interval is  $5 \text{ m s}^{-1}$  for (a),  $1 \text{ m s}^{-1} \text{ K}$  for (b) and  $15 \text{ m}^2 \text{ s}^{-2}$

for (c). The thick black line in **a** and **b** represents the zero contour. The zonal and time average is conducted between  $120^\circ\text{E}$  and  $120^\circ\text{W}$  during winter

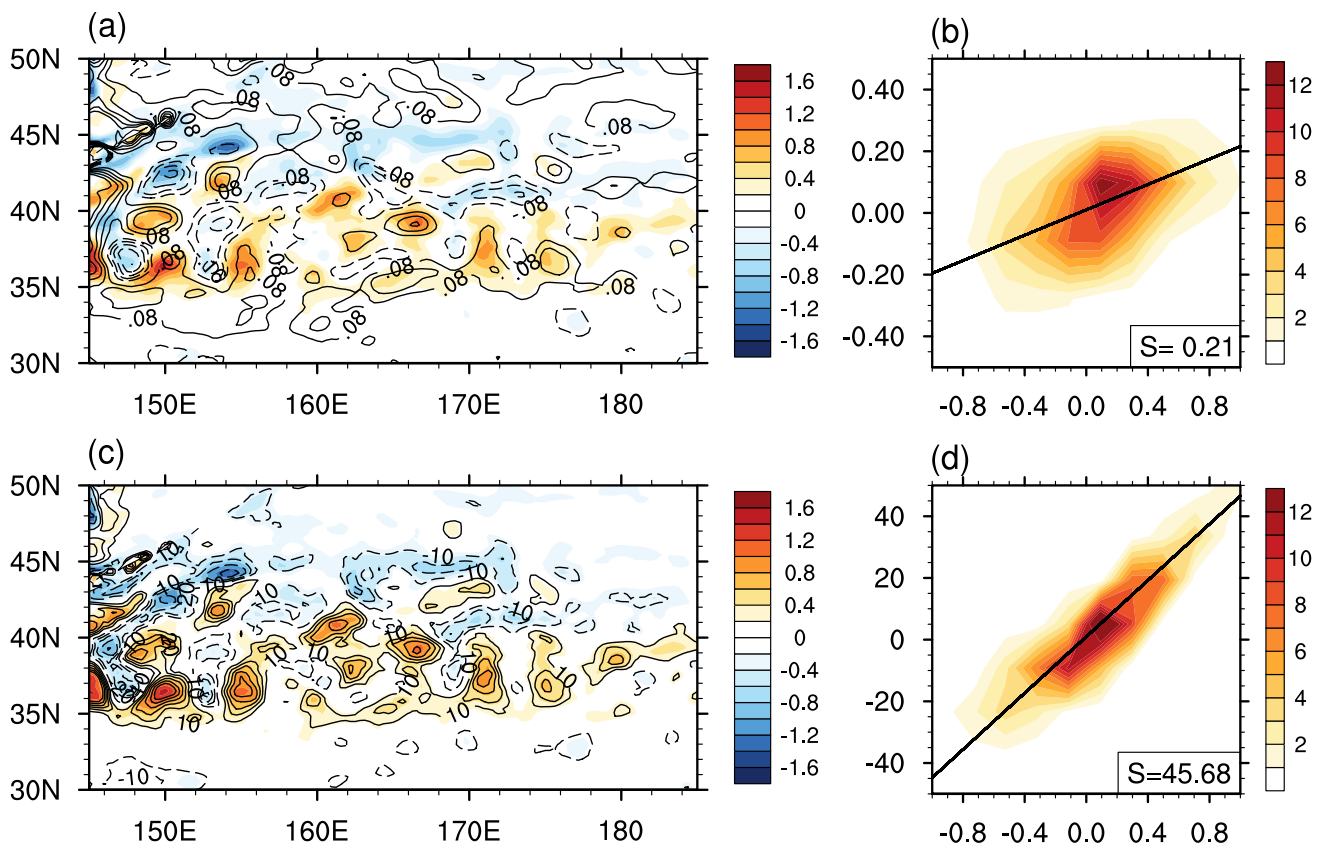


**Fig. 3** **a** Winter mean mesoscale near-surface wind speed (contours; CI=0.08 m s<sup>-1</sup>) and mesoscale SST (shaded). **b** Density plot of mesoscale SST (horizontal axes in °C) and near-surface wind speed (verti-

cal axes, in m s<sup>-1</sup>). **c, d** Same as **a, b** but for mesoscale turbulent heat flux (contours; CI=10 W m<sup>-2</sup>). The black lines in **b** and **d** are the regression lines

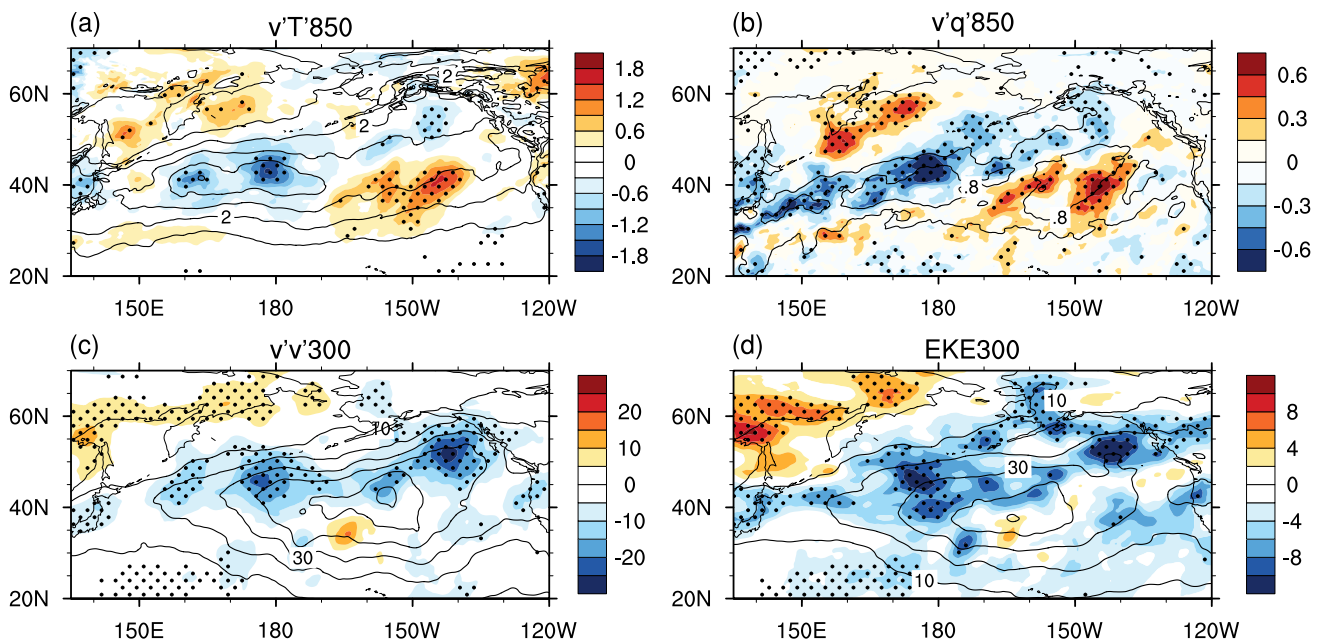
The differences of meridional eddy heat flux at 850 hPa show a significant negative anomaly along KOCR, extending northeast to the Gulf of Alaska, while there is a significant positive anomaly in the eastern North Pacific (Fig. 4a). This result suggests that the storm track decreases along KOCR and shifts southward downstream after removing the mesoscale SST. Meanwhile, the response of meridional eddy specific humidity flux at 850 hPa bears much resemblance with the pattern of meridional eddy heat flux (Fig. 4b), indicating the robust response of storm track. In addition, both the differences of meridional eddy wind variance (Fig. 4c) and EKE at 300 hPa (Fig. 4d) between MSFR and CTRL show a significant decrease extending from KOCR to the Gulf of Alaska, mostly to the north of its climatology position. However, compared with the lower level, the response at upper troposphere seems to be a little different. There is no significant enhancement in the eastern North Pacific.

Figure 5a shows the climatological zonal mean meridional eddy heat flux ( $[\overline{v'T'}]$ ) over KOCR (145°E–180°) in latitude-pressure cross sections of CTRL (contour). The storm track tilts northward from surface to the top troposphere, which was suggested by Booth et al. (2010) and Ma

et al. (2017). The difference (color) between MSFR and CTRL exhibits an approximately 17% decrease against the maximum in CTRL above KOCR in the lower troposphere, indicating that the storm track is greatly influenced by the mesoscale SST. Meanwhile, there is another negative anomaly above 500 hPa, suggesting the substantial impact of the mesoscale SST on the upper troposphere.

Figure 5c shows a similar vertical section plot for meridional eddy wind variance ( $[\overline{v'v'}]$ ). Compared with CTRL, a significant decrease is shown in the upper troposphere, while the anomaly in the lower troposphere is weak and insignificant, which is also associated with the location of climatology of  $[\overline{v'v'}]$  in Fig. 2c. The difference in meridional eddy specific humidity flux ( $[\overline{v'q'}]$ ) is shown in Fig. 5e. After removing the mesoscale SST in MSFR, the meridional eddy specific humidity flux weakens by approximately 24% over KOCR below 700 hPa. These results indicate that the moisture fluxes play an important role in the lower troposphere, while the eddy momentum flux is more sensitive to the mesoscale SST in the upper troposphere.

In addition, the remote response has been investigated. In contrast to the significant decrease in KOCR, the difference



**Fig. 4** The difference (shaded) between MSFR and CTRL in storm track represented by **a** meridional eddy heat flux ( $\text{m s}^{-1} \text{K}$ ), **b** meridional eddy specific humidity flux ( $10^{-3} \text{ m s}^{-1} \text{ kg kg}^{-1}$ ) at 850 hPa, **c** meridional eddy wind variance ( $\text{m}^2 \text{s}^{-2}$ ) and **d** EKE ( $\text{m}^2 \text{s}^{-2}$ ) at

300 hPa. The contours represent the winter mean eddy fluxes in CTRL. Statistically significant differences at 95% according to the bootstrapping test are stippled

in meridional eddy heat flux in the eastern North Pacific (Fig. 5b) exhibits a dipole pattern, with a significant increase to the south and a weak decrease to the north. Similarly, the meridional eddy wind variance (Fig. 5d) and meridional eddy specific humidity flux (Fig. 5f) both show a significant increase at approximately  $40^\circ\text{N}$  in the lower troposphere. These results suggest that the storm track shifts southward downstream after removing the mesoscale SST in MSFR, which is also revealed by Ma et al. (2017). However, the vertical profile of  $[\overline{v'v'}]$  in Ma et al. (2017) shows a local decrease from the surface to the top troposphere and a southward shift in the upper troposphere in the eastern North Pacific, which is different from our results to some extent. This disagreement may arise for many reasons, such as model differences and physical dynamics, which are beyond the scope of this study and will not be discussed in detail.

In general, the comparison between MSFR and CTRL reveals that the response of the storm track to the mesoscale SST shows a significant decrease in the local region and a southward shift downstream in the eastern North Pacific.

## 5 Mechanism of the storm track response

The differences between CTRL and MSFR are only induced by the SST boundary condition. As one may expect, the changes in SST first impact the planetary boundary layer, and the storm track will change only if the impacts can

penetrate into the free atmosphere. Therefore, we investigate the process in the planetary boundary layer and the vertical motion over the KOCR region in this section.

### 5.1 Process in the planetary boundary layer

Figure 6a shows the winter mean surface heat fluxes and precipitation as a function of latitude for CTRL (averaged from  $145^\circ\text{E}$  to  $180^\circ$ ). As shown, most of the region with THF greater than  $200 \text{ W m}^{-2}$  is located within the latitude band between  $30^\circ\text{N}$  and  $45^\circ\text{N}$ , reaching a maximum of around  $300 \text{ W m}^{-2}$  at approximately  $36^\circ\text{N}$ . Note also that the THF is dominated by latent heat flux (LHF), which accounts for 79% in KOCR. The precipitation rate peaks slightly poleward of the maximum THF, reaching  $9 \text{ mm day}^{-1}$ . Figure 6b shows the differences in surface fluxes and precipitation between MSFR and CTRL. The little disturbances of the curves to the north of  $35^\circ\text{N}$  might reflect the influences of mesoscale SST. Compared to CTRL, both sensible and latent heat fluxes decrease by 5% within KOCR in MSFR, while the precipitation exhibits a reduction mainly from  $35^\circ\text{N}$  to  $43^\circ\text{N}$ , reaching  $-0.6 \text{ mm day}^{-1}$ , which is approximately 7% to the maximum in CTRL. These negative anomalies of surface heat flux and precipitation indicates that the mesoscale SST could exert an influence on the planetary boundary layer, reducing the surface heat flux and precipitation over KOCR. In addition, we may notice that the surface heat

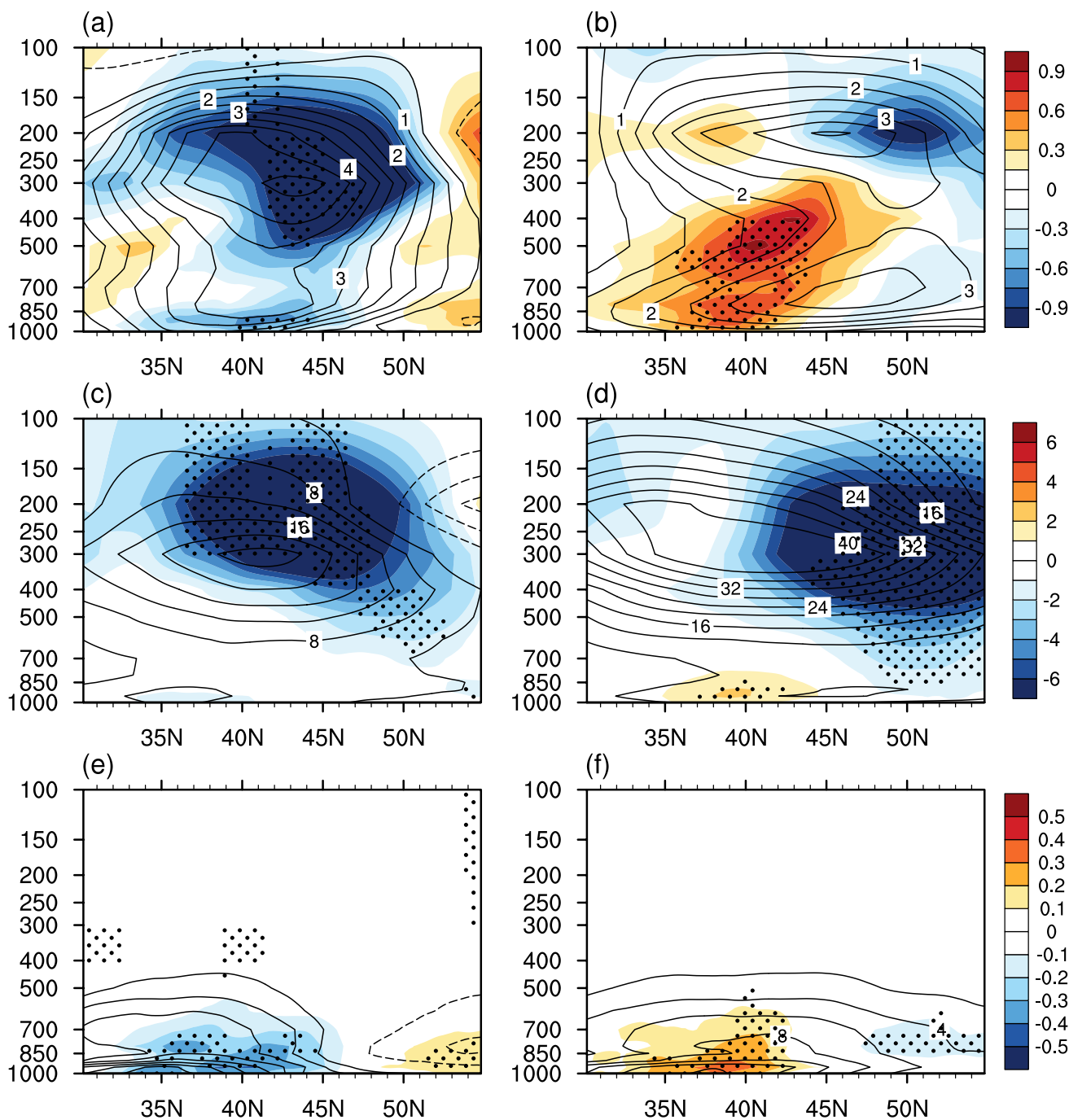


**Fig. 5** Difference in winter mean **a** meridional eddy heat flux ( $v'T'$ ; shaded;  $m\ s^{-1}\ K$ ), **c** meridional eddy wind variance ( $v'v'$ ; shaded;  $m^2\ s^{-2}$ ) and **e** meridional eddy specific humidity flux ( $v'q'$ ; shaded;  $10^{-3}\ kg\ kg^{-1}$ ) between MSFR and CTRL simulations over the western North Pacific (averaged from  $140^\circ E$  to  $180^\circ$ ). **b**, **d**, **f** Same as **a**, **c**,

**e** but for the eastern North Pacific ( $170^\circ W$  to  $130^\circ W$ ). The contours stand for the winter mean eddy fluxes in CTRL, with contour intervals of  $0.5\ m\ s^{-1}\ K$  in **a**, **b**,  $4\ m^2\ s^{-2}$  in **c**, **d**, and  $2 \times 10^{-4}\ kg\ kg^{-1}$  in **(e)**, **(f)**. Statistically significant differences at the 90% confidence interval according to the bootstrapping test are stippled

flux and precipitation increase to the south of  $35^\circ N$ . This may be associated with the response to changes in SST. Although the large-scale SST barely changes, removing mesoscale SST in MSFR still leads to a cyclonic response to the south of Japan, associated with an upward and

southward motion (not shown). This response further contributes to the enhancement of THF and precipitation to the south of  $35^\circ N$ .

To further investigate the mesoscale response in the boundary layer, we applied the high-pass spatial boxcar

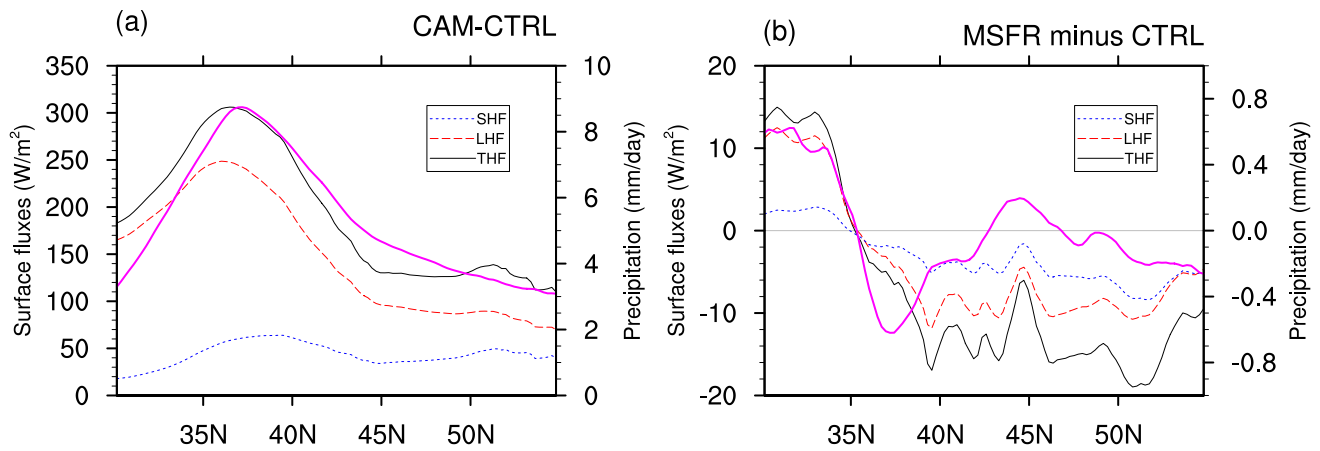


**Fig. 6** **a** Zonal and time averaged surface heat fluxes ( $W m^{-2}$ ) and precipitation ( $mm day^{-1}$ ) in CTRL. **b** Same as **a** but for the difference between MSFR and CTRL. The zonal and time average is conducted

between  $140^{\circ}E$  and  $180^{\circ}E$  during winter (ONDJF). The black, blue, red and magenta lines represent the turbulent heat flux, sensible heat flux, latent heat flux and precipitation, respectively

filter ( $5^{\circ} \times 5^{\circ}$ ) on both THF and planetary boundary layer height (PBLH) in MSFR and CTRL (Fig. 7). As shown, the mesoscale THF is closely related to mesoscale SST in CTRL, with a pattern correlation coefficient reaching 0.79 in KO CR (Fig. 7a). By contrast, there are no mesoscale structures emerging in THF in MSFR due to the lack of mesoscale SST (Fig. 7b). That is, resolving the small structures of SST could greatly impact the THF. In particular, the warm mesoscale SST anomalies are stronger than the cold ones, which leads to larger positive anomalies in mesoscale THF

than negative THF anomalies (Fig. 7a). Liu et al. (2018) revealed that the influence of oceanic warm and cold eddies was asymmetric. Their results showed that the atmospheric response to the mesoscale warm eddies was considerably stronger than the response to cold oceanic eddies. Foussard et al. (2019) also indicated that the net and positive surface heating of the atmosphere was induced by eddy-induced SST anomalies. Associated with the anomalies in THF, the mesoscale PBLH overlaid on the mesoscale SST in CTRL and MSFR is shown in Fig. 7c, d, respectively. In CTRL,

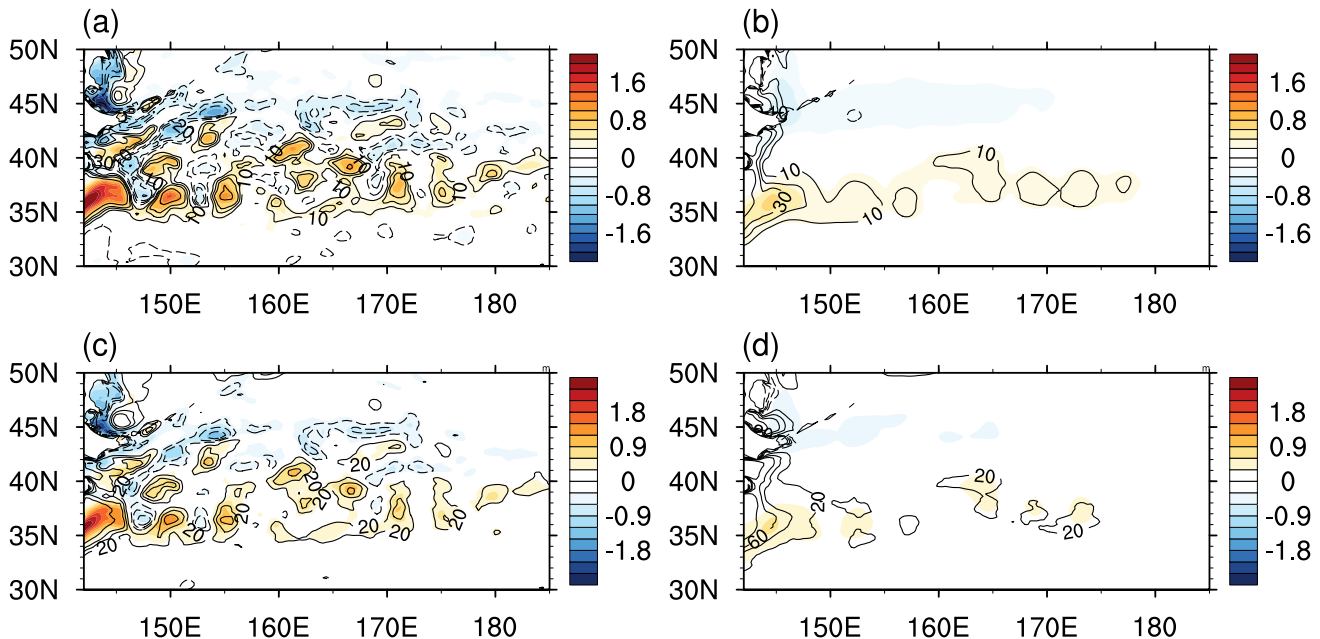


**Fig. 7** Winter mean **a** mesoscale THF (contours;  $CI=10 W m^{-2}$ ) and **c** PBLH (contours;  $CI=20 m$ ) overlaid on the mesoscale SST (shaded; units:  $^{\circ}C$ ) in CTRL. **b**, **d** Same as **a**, **c** but in MSFR



a strong and positive correlation ( $\sim 0.69$ ) indicates a close relationship between mesoscale SST and PBLH, while the pattern correlation coefficient is only 0.32 in MSFR, and no mesoscale features could be found.

Then, we investigate the response of convergence to the mesoscale SST. As indicated by previous studies, two mechanisms, known as the pressure adjustment mechanism (PAM; Lindzen and Nigam 1987) and vertical momentum mixing (VMM; Wallace et al. 1989), are proposed to explain the response of near-surface convergence. By PAM, the near-surface convergence is proportional to the Laplacian of sea level pressure (SLP) (Minobe et al. 2008; Takatama et al. 2012), while the VMM indicates that the downward momentum transport induced by instability of the atmosphere would accelerate surface winds over the SST gradient (Chen et al. 2017). Liu et al. (2013) and Chen et al. (2017) have suggested that PAM and VMM may depend on the time scale and that the PAM prevails at longer time scales more than a month, while VMM is dominant at synoptic variation.

As indicated by Fig. 7, the mesoscale imprints on THF are only found in CTRL and the difference between MSFR and CTRL is shown in Fig. 8a. Positive (negative) mesoscale THF anomalies are overlaid over warm (cold) mesoscale SSTs. The pattern correlation coefficient is up to 0.97 over

the region ( $35^{\circ}\text{N}$ – $45^{\circ}\text{N}$ ,  $145^{\circ}\text{E}$ – $180^{\circ}\text{E}$ ). More (less) heat out of the ocean over positive (negative) mesoscale SSTs further warms (cools) the atmosphere near surface (Fig. 8b). The correlation coefficient between mesoscale THF and mesoscale air temperature (AT) at surface is 0.78. These results suggest that the mesoscale SST can lead to changes of thermal structure of the atmospheric boundary layer through THF. Figure 8c shows that there is a fair correspondence between SLP Laplacian and mesoscale AT at surface (correlation coefficient of 0.65), which indicates that the anomalies of AT lead to the changes of SLP. Further, the wind speed at surface is altered under the pressure gradient (not shown). The spatial pattern of the differences in Laplacian of SLP and in convergence bears much similarity, with the correlation coefficient up to 0.69 in KOCR (Fig. 8d).

Based on these results, we found that the PAM was primarily responsible for the surface convergence differences. Firstly, the mesoscale SST impacts on the air temperature through the surface heat fluxes (Fig. 8a). Then, the changes in air temperature alter the local SLP, and then the pressure gradient. The large spatial correlation coefficient between the SLP Laplacian and mesoscale air temperature (0.65) demonstrated the relationship between mesoscale SST anomalies and SLP anomalies (Fig. 8c). Finally, the change

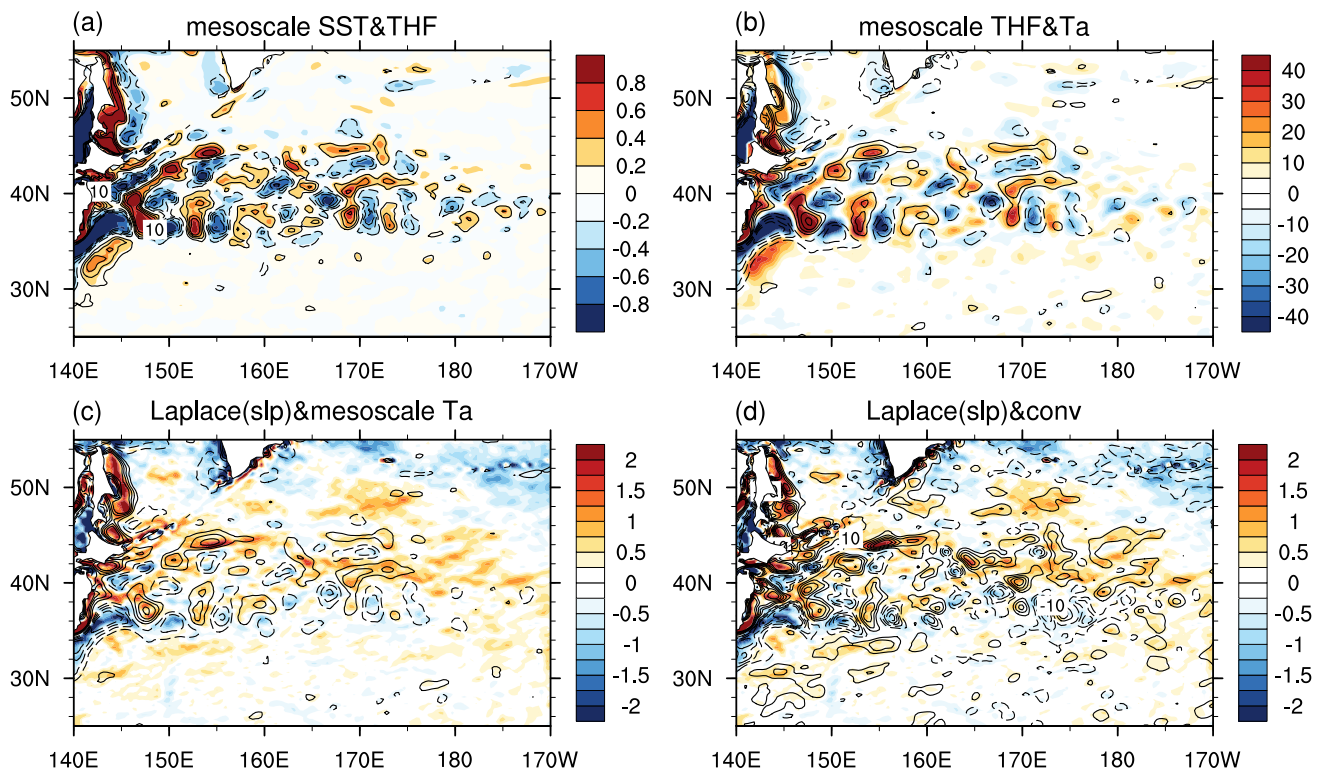


**Fig. 8** **a** The difference of mesoscale SST (shaded; units:  $^{\circ}\text{C}$ ) and turbulent heat flux (THF;  $\text{CI}=10 \text{ W m}^{-2}$ ) between MSFR and CTRL simulations. **b** Same as **(a)** but for mesoscale THF (shaded; units:  $\text{W m}^{-2}$ ) and mesoscale air temperature ( $\text{Ta}$ ;  $\text{CI}=0.05 \text{ }^{\circ}\text{C}$ ) at surface. **c**

Same as **(a)**, but for Laplacian of SLP (shaded; units =  $10^{-9} \text{ Pa m}^{-2}$ ) and mesoscale  $\text{Ta}$  ( $\text{CI}=0.05 \text{ }^{\circ}\text{C}$ ). **d** Same as **(a)** but for Laplacian of SLP (shaded; units =  $10^{-9} \text{ Pa m}^{-2}$ ) and convergence ( $\text{CI}=1 \times 10^{-6} \text{ s}^{-1}$ ) at surface. For clarity, the zero contour is omitted in all plots

in pressure gradient could drive the changes in the surface wind and cause the differences of convergence/divergence near surface. Koseki and Watanabe (2010) has shown the contribution of PAM and VMM can be comparable in Kuroshio Extension region in January. In our case, however, we could not find clear signals related with VMM.

## 5.2 Vertical motion

To further examine the influence of mesoscale SST on the atmosphere and understand the process that connects the boundary layer and free troposphere, we show the vertical motion driven by the near-surface convergence/divergence in Fig. 9. The profiles are averaged between 35°N and 40°N instead of a single latitude to reflect a mean state over KOCR. The negative (positive) anomalies of vertical velocity represent the downward (upward) motion, which are located over the near-surface convergence (divergence) near 146°E, 152°E and 156°E (148°E, 154°E and 159°E). It is clear that after removing the mesoscale SST in MSFR, the vertical upward air motion is suppressed. We found that the strong negative vertical anomalies could penetrate as high as 700 hPa at both 146°E and 152°E, and form secondary circulation cells over KOCR.

Figure 10 shows the difference in vertical eddy heat flux ( $\overline{(\omega'T')}$ ) and specific humidity flux ( $\overline{(\omega'q')}$ ). As shown, a significant decrease exists in KOCR, which indicates that less heat and moisture are transported from the bottom to the top troposphere in MSFR. This result is also in good agreement with Jia et al. (2019) that the vertical moisture fluxes can be enhanced by oceanic eddies. Besides, this result may lead to the stable atmosphere through less latent heat release.

## 5.3 Baroclinicity and energy conversion

As noted by previous studies, the development of storm track is in good agreement with the variation in baroclinicity in the lower troposphere (Nakamura et al. 2004, 2008; Joyce et al. 2009). Commonly, the baroclinicity can be represented by the maximum Eady growth rate (EGR; Hoskins and Valdes 1990; Kuwano-Yoshida and Minobe 2017). The EGR is defined as:

$$\text{EGR} = 0.31 \frac{f}{N} \left| \frac{\partial u}{\partial z} \right| = 0.31 \frac{g}{N\theta} \left| \frac{\partial \theta}{\partial y} \right| \quad (1)$$

where  $N = \sqrt{\frac{g}{\theta} \frac{\partial \theta}{\partial z}}$  is the Brunt-Väisälä frequency,  $g$  is the gravitational acceleration,  $f$  is the Coriolis parameter, and  $u$  is the zonal wind velocity. Figure 11a shows the differences in EGR between MSFR and CTRL. After removing the mesoscale SST in MSFR, the EGR decreases over western North Pacific and increases downstream. It is clear that the changes of meridional eddy heat flux are over regions where EGR is

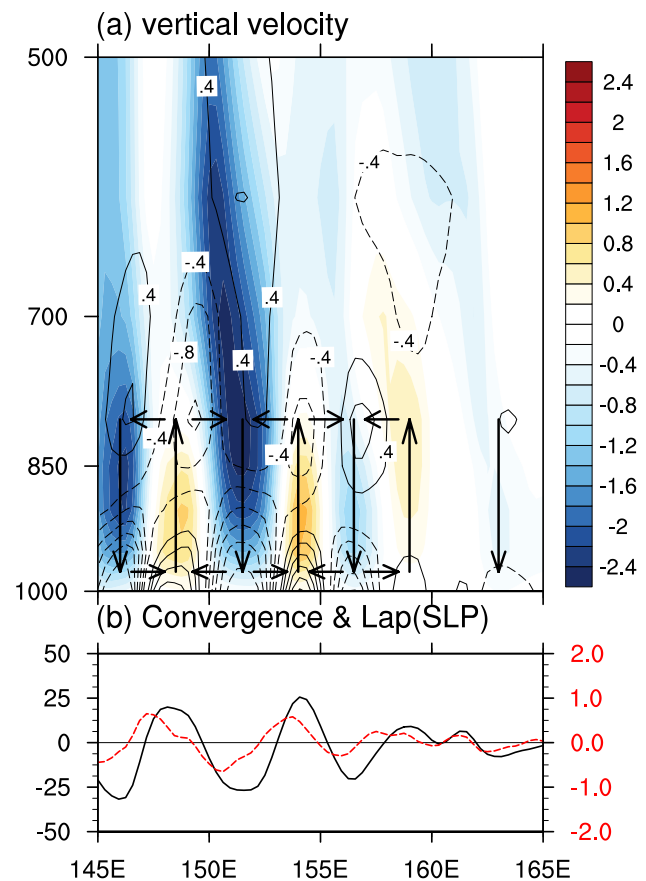


**Fig. 9** **a** Vertical profile of the differences in vertical velocity (shaded; positive upward;  $10^{-2} \text{ Pa s}^{-1}$ ) and convergence/divergence ( $\text{CI} = 5 \times 10^{-7} \text{ s}^{-1}$ ) between MSFR and CTRL averaged between 35°N and 40°N. **b** The differences in convergence/divergence ( $10^{-7} \text{ s}^{-1}$ ; black line) and Laplacian SLP ( $10^{-9} \text{ Pa m}^{-2}$ ; red dashed line) between MSFR and CTRL averaged between 35°N and 40°N. The arrows in (a) depict the schematic of secondary anomalous circulation induced by mesoscale SST above KOCR

increased or decreased, which suggests its important role in modulating the storm track.

To understand the changes of EGR, we further examined the vertical shear of zonal velocity ( $u$ ) and  $N$  following the Eq. (1). Meanwhile, according to the thermal wind equation, the EGR is also proportional to the meridional gradient of potential temperature. Filtering out the mesoscale SST in MSFR directly influenced on the THF as shown in Fig. 11b. The negative anomalies over KOCR and north-west North Pacific demonstrate that there is less heat out of the ocean in MSFR, which could decrease the air temperature and increase the static stability of lower troposphere in this region (Fig. 11c). In Sects. 5.1 and 5.2, we have shown that the differences in boundary layer due to mesoscale SST result in changes in near-surface convergence/divergence, forming a secondary air circulation through PAM over KOCR (Fig. 9). The value of negative anomalies is

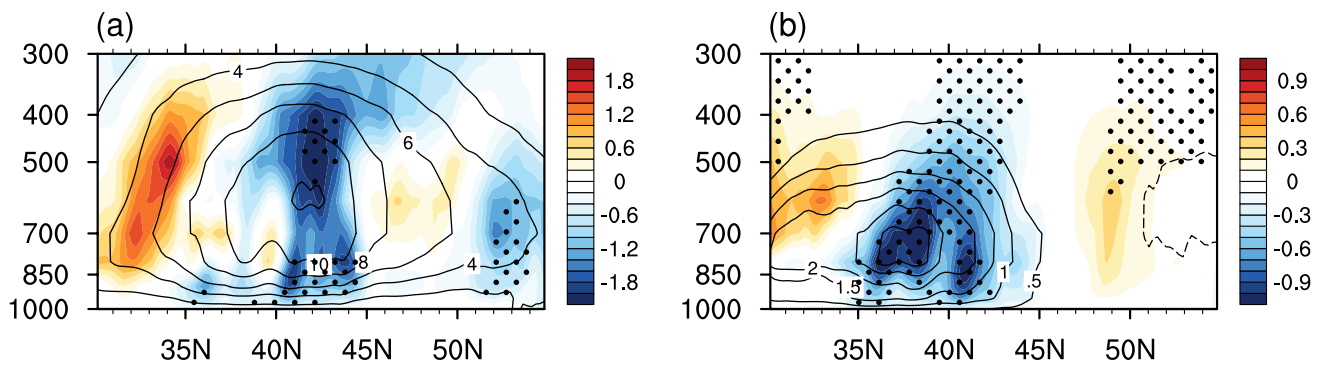


**Fig. 10** Difference in winter mean **a** vertical eddy heat flux ( $\omega'T'$ ; positive upward; shaded;  $10^{-2}$  Pa  $s^{-1}$  K) and **b** vertical eddy specific humidity flux ( $\omega'q'$ ; positive upward; shaded;  $10^{-5}$  Pa  $s^{-1}$  kg  $kg^{-1}$ ) between MSFR and CTRL simulations over the western North

Pacific (averaged from 145°E to 180°). The contours represent the winter mean eddy fluxes in CTRL, with a contour interval of  $2 \times 10^{-2}$  Pa  $s^{-1}$  K in **(a)** and  $5 \times 10^{-6}$  Pa  $s^{-1}$  kg  $kg^{-1}$  in **(b)**. Statistically significant differences at the 90% confidence interval according to the bootstrapping test are stippled

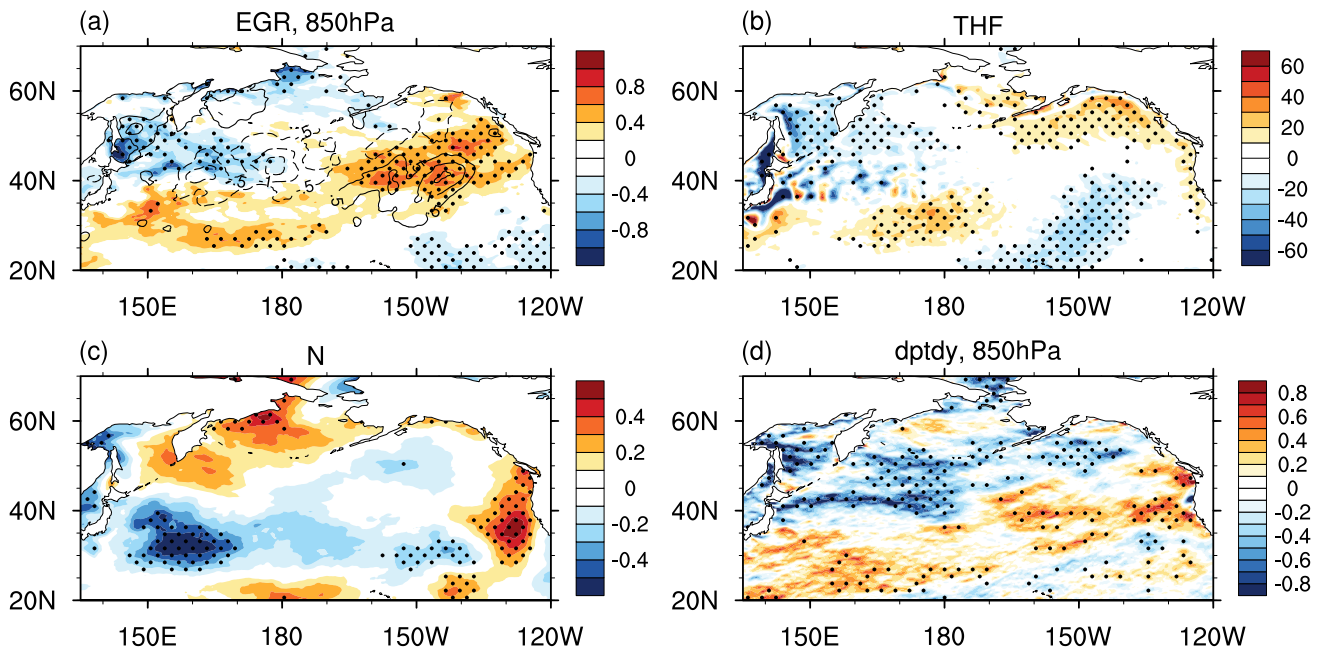


**Fig. 11** The difference of winter mean **a** EGR (units:  $10^{-6}$   $s^{-1}$ ), **b** THF (positive upward; units:  $W m^{-2}$ ), **c**  $N$  ( $10^{-3}$   $s^{-1}$ ) and **d** meridional gradient of potential temperature ( $d\theta/dy$ ; units:  $10^{-6}$  K  $m^{-1}$ ) at

850 hPa between MSFR and CTRL simulations. Statistically significant differences at the 90% confidence interval according to the bootstrapping test are stippled

significantly larger than the positive one, which means that the vertical motion is greatly suppressed in MSFR. Meanwhile, Fig. 10a shows significant differences of vertical eddy heat flux over KOCCR, indicating that removing the mesoscale SST in MSFR further leads to less heat transport from the surface to the troposphere by transient eddies. Less heat release and suppressed vertical motion are in favor of the homogeneous temperature and flow fields, which may be responsible for the decrease of the meridional temperature gradient (Fig. 11d). Increasing static stability and decreasing

meridional gradient of temperature finally contribute to the decrease in EGR or the baroclinicity of troposphere in this region.

Due to the decrease of EGR over western North Pacific, the transient eddies developed slowly in MSFR and saturated downstream eastern North Pacific, perturbing the air and strengthening the temperature gradient. This may lead to stronger EGR downstream. Ma et al. (2017) has shown that the downstream influence of mesoscale SST can be due to the transient eddy feedback. Overall, mesoscale SST firstly

influence the surface heat fluxes and then the vertical motion which connects the surface and the free atmosphere, causing the redistribution of heat in the atmosphere and finally reducing the local atmospheric baroclinicity.

Subsequently, we examined the energy conversion at 850 hPa, which includes barotropic kinetic energy conversion (BTEC) and baroclinic energy conversion (BCEC). The former is from mean flow kinetic energy (MKE) to eddy kinetic energy (EKE). The latter consists two parts. One is the energy conversion from the mean available potential energy (MAPE) to the eddy available potential energy (EAPE) and the other is from EAPE to EKE, denoted as BCEC1 and BCEC2, respectively. Following Cai et al. (2007) and Gan and Wu (2013), the BTEC and BCEC can be expressed as:

$$BTEC = C_0 \left[ \frac{1}{2} (\overline{v^2} - \overline{u^2}) + (-\overline{u'v'}) \left( \frac{\partial \overline{v}}{\partial x} + \frac{\partial \overline{u}}{\partial y} \right) \right] \quad (2)$$

$$BCEC1 = -C_1 \left( \frac{P_0}{p} \right)^{\frac{R}{C_p}} \left( -\frac{d\theta}{dp} \right)^{-1} \left( \overline{u'T'} \frac{\partial \overline{T}}{\partial x} + \overline{v'T'} \frac{\partial \overline{T}}{\partial y} \right) \quad (3)$$

$$BCEC2 = -C_1 \overline{(\omega'T')} \quad (4)$$

where  $C_0 = \frac{P_0}{g}$ ,  $C_1 = \left( \frac{P_0}{p} \right)^{\frac{C_p}{R}} \frac{R}{g}$ , and  $R$ ,  $\omega$ ,  $\theta$ ,  $C_p$  and  $C_v$  represent the gas constant for dry air, vertical velocity, potential temperature, and the specific heat capacity of dry air at constant pressure and at constant volume, respectively. The overbar and prime denote time mean and synoptic-scale disturbance. The response of BTEC is much smaller in magnitude than BCEC (not shown). Therefore, we mainly examine the changes in BCEC. Figure 12a, b shows the differences in BCEC1 and BCEC2 between MSFR and CTRL, respectively. In contrast to the differences in EGR, a significant decrease in BCEC1 appears between 160°E and 180°, close to the negative anomaly of the storm track, reducing

the EAPE transferred from MAPE. Meanwhile, the strengthening BCEC1 over the east North Pacific indicates more energy is converted to the eddy potential energy. The changes in BCEC1 further contribute to the anomalies of BCEC2, which exhibit a very close relationship with the spatial pattern of the differences in the storm track, with a decrease along the KOCR region extending towards the Gulf of Alaska, as well as an increase over the eastern North Pacific. The pattern correlation coefficient is 0.47 for BCEC1 and 0.53 for BCEC2. From the results above, we may argue that the baroclinicity and BCEC play a key role in modulating the storm track response to mesoscale SST.

### 6 Conclusions

The North Pacific storm track response to mesoscale SST is investigated using a high-resolution CAM4 model. Two simulations forced by eddy-resolving SST and eddy-filtered-out SST are conducted. Compared with the ERA-Interim and previous studies, the model is confirmed to have a reasonable representation of the storm track climatology and the responses of surface atmosphere to mesoscale SST are well simulated. After removing the mesoscale SST, the meridional eddy heat flux and meridional eddy specific humidity flux at 850 hPa show a significant decrease along KOCR and a significant increase in eastern North Pacific. Further insight into the vertical structure of the responses, the significant decrease (~20%) in the lower troposphere over western North Pacific can also be found. In the remote region, a dipole structure is identified in meridional eddy heat flux and meridional specific humidity flux. These results suggest that the storm track significantly decreases along KOCR and shifts southward downstream, which shows a good agreement with Ma et al. (2015, 2017). Thus, we suspect that the difference in a regional and global model is not essential to the influence on the storm track. That is, the changes due to the mesoscale SST variability in other regions, such as the

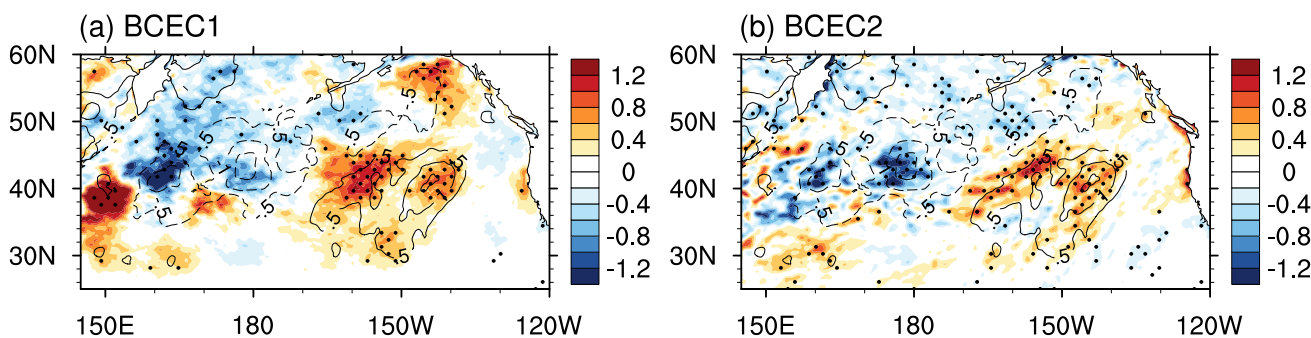


**Fig. 12** Differences between MSFR and CTRL of the **a** BCEC1 (shaded;  $W m^{-2}$ ) and **b** BCEC2 (shaded;  $W m^{-2}$ ) at 850 hPa. Black contours show the differences in storm track represented by meridional eddy heat flux ( $CI=0.5 m s^{-1} K$ ) at 850 hPa. For clarity, the zero contour is omitted. Statistically significant differences at the 95% confidence interval according to the bootstrapping test are stippled

North Atlantic, do not significantly affect the storm track in the North Pacific. Nevertheless, we still argue that the regional influence on the storm track should be investigated further.

Then, we establish the relationship between the response in the boundary layer and the response of the storm track in the free atmosphere. The process can be summarized as follows. First, the only difference between CTRL and MSFR is the SST conditions, and due to the lack of mesoscale SST, the surface heat fluxes decrease in MSFR, leading to changes in the thermal structures of the boundary layer. Next, the convergence induced by the PAM is altered, forcing a secondary circulation along KOCR. Subsequently, the vertical eddy heat and specific humidity fluxes decrease in MSFR, which reduces heat and moisture into free troposphere. Less heat into the troposphere further leads to weaker meridional temperature gradient and stronger static stability, which further contribute to the decrease in the baroclinicity of troposphere in this region. In addition, the energy conversion process has been investigated. The changes of baroclinic energy conversion, bear much resemblance with the anomalies of storm track, modulating the response of storm track to the mesoscale SST. Finally, the activities of storms are suppressed, associated with a reduction in precipitation in MSFR. From the results above, we highlight the response of vertical motion to the mesoscale SST. Only the response in the boundary layer that generates upward motion extending to the free atmosphere can influence the storm track. These results agree with previous studies (Minobe et al. 2008; Small et al. 2008; Tokinaga et al. 2009; Jia et al. 2019), which shows that the frontal and mesoscale structures of western boundary currents could exert a deep impact on the troposphere.

Overall, this study contributes to our understanding of the mechanism of storm track and the air–sea interaction at middle latitudes. We also note that the resolution in simulating the storm track is important. To better represent the storm track, we suggest a high-resolution model at either a regional or a global scale. In addition, the oceanic forcing in the atmospheric model is one way, which disagrees with the actual air–sea interaction. Thus, a fully coupled model should be applied to examine the response of the storm track.

**Acknowledgements** This study is supported by the National Natural Science Foundation of China (Grant Nos. 41490642, 41576025, 41776030 and 41806034). We appreciate three reviewers for their suggestions to improve the manuscript substantially.

## References

- Alexander MA, Bladé I, Newman M, Lanzante JR, Lau NC, Scott JD (2002) The atmospheric bridge: the influence of ENSO teleconnections on air–sea interaction over the global oceans. *J Clim* 15:2205–2231. [https://doi.org/10.1175/1520-0442\(2002\)015<2205:TABTIO>2.0.CO;2](https://doi.org/10.1175/1520-0442(2002)015<2205:TABTIO>2.0.CO;2)
- Bishop SP, Small RJ, Bryan FO, Tomas RA (2017) Scale dependence of midlatitude air–sea interaction. *J Clim* 30:8207–8221. <https://doi.org/10.1175/JCLI-D-17-0159.1>
- Booth JF, Thompson LA, Patoux J, Kelly KA, Dickinson S (2010) The signature of the midlatitude tropospheric storm tracks in the surface winds. *J Clim* 23:1160–1174. <https://doi.org/10.1175/2009JCLI3064.1>
- Booth JF, Kwon YO, Ko S, Small RJ, Msadek R (2017) Spatial patterns and intensity of the surface storm tracks in CMIP5 models. *J Clim* 30:4965–4981. <https://doi.org/10.1175/JCLI-D-16-0228.1>
- Bryan FO, Tomas RA, Dennis JM, Chelton DB, Loeb NG, McClean JL (2010) Frontal scale air–sea interaction in high-resolution coupled climate models. *J Clim* 23:6277–6291. <https://doi.org/10.1175/2009JCLI3064.1>
- Cai M, Yang S, Dool H, Kousky VE (2007) Dynamical implications of the orientation of atmospheric eddies: a local energetics perspective. *Tellus A* 59:127–140. <https://doi.org/10.1111/j.1600-0870.2006.00213.x>
- Chang EKM, Lee S, Swanson KL (2002) Storm track dynamics. *J Clim* 15:2163–2183. [https://doi.org/10.1175/1520-0442\(2002\)015<02163:STD>2.0.CO;2](https://doi.org/10.1175/1520-0442(2002)015<02163:STD>2.0.CO;2)
- Chelton DB, Schlax MG, Freilich MH, Milliff RF (2004) Satellite measurements reveal persistent small-scale features in ocean winds. *Science* 303:978. <https://doi.org/10.1126/science.1091901>
- Chen L, Jia Y, Liu Q (2017) Oceanic eddy-driven atmospheric secondary circulation in the winter Kuroshio Extension region. *J Oceanogr* 73:295–307. <https://doi.org/10.1007/s10872-016-0403-z>
- Chu C, Hu H, Yang XQ (2020) Midlatitude atmospheric transient eddy feedbacks influenced enso-associated wintertime pacific teleconnection patterns in two PDO phases. *Clim Dyn* 54:257–2595. <https://doi.org/10.1007/s00382-020-05134-4>
- Dee DP, Uppala SM, Simmons AJ, Berrisford P, Poli P, Kobayashi S et al (2011) The ERA-Interim reanalysis: configuration and performance of the data assimilation system. *Q J R Meteorol Soc* 137:553–597. <https://doi.org/10.1002/qj.828>
- Feliks Y, Ghil M, Simonnet E (2004) Low-frequency variability in the midlatitude atmosphere induced by an oceanic thermal front. *J Atmos Sci* 61:961–981. [https://doi.org/10.1175/1520-0469\(2004\)061<0961:LVITMA>2.0.CO;2](https://doi.org/10.1175/1520-0469(2004)061<0961:LVITMA>2.0.CO;2)
- Foussard A, Lapeyre G, Plougonven R (2018) Storm track response to oceanic eddies in idealized atmospheric simulations. *J Clim* 32:445–463. <https://doi.org/10.1175/JCLI-D-18-0415.1>
- Foussard A, Lapeyre G, Plougonven R (2019) Response of surface wind divergence to mesoscale SST anomalies under different wind conditions. *J Atmos Sci*. <https://doi.org/10.1175/JAS-D-18-0204.1>
- Frankignoul C, Sennéchal N, Kwon YO, Alexander MA (2011) Influence of the meridional shifts of the Kuroshio and the Oyashio extensions on the atmospheric circulation. *J Clim* 24:762–777. <https://doi.org/10.1175/2010JCLI3731.1>
- Frenger I, Gruber N, Knutti R, Munnich M (2013) Imprint of Southern Ocean eddies on winds, clouds and rainfall. *Nat Geosci* 6:608–612. <https://doi.org/10.1038/ngeo1863>
- Gan B, Wu L (2013) Seasonal and long-term coupling between wintertime storm tracks and sea surface temperature in the North Pacific. *J Clim* 26:6123–6136. <https://doi.org/10.1175/JCLI-D-12-00724.1>
- Hoskins BJ, Valdes PJ (1990) On the existence of storm-tracks. *J Atmos Sci* 47:1854–1864. [https://doi.org/10.1175/1520-0469\(1990\)047<1854:OTEOST>2.0.CO;2](https://doi.org/10.1175/1520-0469(1990)047<1854:OTEOST>2.0.CO;2)
- Hoskins BJ, Hodges KI (2002) New Perspectives on the Northern Hemisphere Winter Storm Tracks. *J Atmos Sci* 59:1041–1061. [https://doi.org/10.1175/1520-0469\(2002\)059<1041:NPOTNH>2.0.CO;2](https://doi.org/10.1175/1520-0469(2002)059<1041:NPOTNH>2.0.CO;2)
- Jia Y, Chang P, Szunyogh I, Saravanan R, Bacmeister JT (2019) A modeling strategy for the investigation of the effect of

- mesoscale SST variability on atmospheric dynamics. *Geophys Res Lett* 46:3982–3989. <https://doi.org/10.1029/2019GL081960>
- Joyce TM, Kwon Y, Yu L (2009) On the relationship between synoptic wintertime atmospheric variability and path shifts in the Gulf Stream and the Kuroshio Extension. *J Clim* 22:3177–3192. <https://doi.org/10.1175/2008JCLI2690.1>
- Koseki S, Watanabe M (2010) Atmospheric boundary layer response to mesoscale SST anomalies in the kuroshio extension. *J Climate* 23:2492–2507. <https://doi.org/10.1175/2009JCLI2915.1>
- Kuwano-Yoshida A, Minobe S (2017) Storm-track response to SST fronts in the Northwestern Pacific Region in an AGCM. *J Climate* 30:1081–1102. <https://doi.org/10.1175/JCLI-D-16-0331.1>
- Lau NC, Nath MJ (1991) Variability of the baroclinic and barotropic transient eddy forcing associated with monthly changes in the midlatitude storm tracks. *J Atmos Sci* 48:2589–2613. [https://doi.org/10.1175/1520-0469\(1991\)048<2589:VOTBA>2.0.CO;2](https://doi.org/10.1175/1520-0469(1991)048<2589:VOTBA>2.0.CO;2)
- Lee S, Kim H (2003) The dynamical relationship between subtropical and eddy-driven jets. *J Atmos Sci* 60:1490–1503. [https://doi.org/10.1175/1520-0469\(2003\)060<1490:TDRBSA>2.0.CO;2](https://doi.org/10.1175/1520-0469(2003)060<1490:TDRBSA>2.0.CO;2)
- Lin P, Liu H, Ma J, Li Y (2019) Ocean mesoscale structure-induced air–sea interaction in a high-resolution coupled model. *Atmos Ocean Sci Lett* 12:98–106. <https://doi.org/10.1080/16742834.2019.1569454>
- Lindzen RS, Nigam S (1987) On the role of sea surface temperature gradients in forcing low-level winds and convergence in the tropics. *J Atmos Sci* 44:2418–2436. [https://doi.org/10.1175/1520-0469\(1987\)044<2418:OTROSS>2.0.CO;2](https://doi.org/10.1175/1520-0469(1987)044<2418:OTROSS>2.0.CO;2)
- Liu JW, Zhang SP, Xie SP (2013) Two Types of Surface Wind Response to the East China Sea Kuroshio Front. *J Clim* 26:8616–8627. <https://doi.org/10.1175/JCLI-D-12-00092.1>
- Liu X, Chang P, Kurian J, Saravanan R, Lin X (2018) Satellite-observed precipitation response to ocean mesoscale eddies. *J Climate* 31:6879–6895. <https://doi.org/10.1175/JCLI-D-17-0668.1>
- Ma X, Chang P, Saravanan R, Montuoro HJ, Wu D et al (2015) Distant influence of Kuroshio Eddies on North Pacific weather patterns? *Sci Rep* 5:17785. <https://doi.org/10.1038/srep17785>
- Ma X, Chang P, Saravanan R, Montuoro R, Nakamura H, Wu D et al (2017) Importance of resolving Kuroshio front and eddy influence in simulating the North Pacific storm track. *J Clim* 30:1861–1880. <https://doi.org/10.1175/JCLI-D-16-0154.1>
- Masunaga R, Nakamura H, Miyasaka T, Nishii K, Tanimoto Y (2015) Separation of climatological imprints of the Kuroshio extension and Oyashio fronts on the wintertime atmospheric boundary layer: their sensitivity to SST resolution prescribed for atmospheric reanalysis. *J Clim* 28:1764–1787. <https://doi.org/10.1175/JCLI-D-14-00314.1>
- Masunaga R, Nakamura H, Miyasaka T, Nishii K, Qiu B (2016) Interannual modulations of oceanic imprints on the wintertime atmospheric boundary layer under the changing dynamical regimes of the Kuroshio extension. *J Clim* 29:3273–3296. <https://doi.org/10.1175/JCLI-D-15-0545.1>
- Minobe S, Kuwano-Yoshida A, Komori N, Xie S-P, Small RJ (2008) Influence of the Gulf Stream on the troposphere. *Nature* 452:206. <https://doi.org/10.1038/nature06690>
- Nakamura H, Sampe T, Tanimoto Y, Shimpo A (2004) Observed associations among storm tracks, jet streams and midlatitude oceanic fronts. *Earth's Climate: The Ocean-Atmosphere Interaction*. Geophys. Monogr., vol 147. American Geophysical Union, pp329–346. <https://doi.org/10.1029/147GM18>
- Nakamura H, Sampe T, Goto A, Ohfuchi W, Xie S-P (2008) On the importance of midlatitude oceanic frontal zones for the mean state and dominant variability in the tropospheric circulation. *Geophys Res Lett* 35:L15709. <https://doi.org/10.1029/2008GL034010>
- Neale RB, Richter J, Park S, Lauritzen PH, Vavrus SJ, Rasch PJ, Zhang M (2013) The mean climate of the community atmosphere model (CAM4) in forced SST and fully coupled experiments. *J Clim* 26:5150–5168. <https://doi.org/10.1175/JCLI-D-12-00236.1>
- Parfitt R, Czaja A, Kwon YO (2017) The impact of SST resolution change in the ERA-Interim reanalysis on wintertime Gulf Stream frontal air–sea interaction. *Geophys Res Lett* 44:3246–3254. <https://doi.org/10.1002/2017GL073028>
- Piazza M, Terray L, Boé J, Maisonnave E, Sanchez-Gomez E (2016) Influence of small-scale North Atlantic sea surface temperature patterns on the marine boundary layer and free troposphere: a study using the atmospheric ARPEGE model. *Clim Dyn* 46:1699–1717. <https://doi.org/10.1007/s00382-015-2669-z>
- Révelard A, Frankignoul C, Sennéchal N, Kwon YO, Qiu B (2016) Influence of the decadal variability of the Kuroshio extension on the atmospheric circulation in the cold season. *J Clim* 29:2123–2144. <https://doi.org/10.1175/JCLI-D-15-0511.1>
- Sampe T, Nakamura H, Goto A, Ohfuchi W (2010) Significance of a midlatitude SST frontal zone in the formation of a storm track and an eddy-driven westerly jet. *J Clim* 23:1793–1814. <https://doi.org/10.1175/2009JCLI3163.1>
- Seager R, Naik N, Ting M, Cane M, Harnik N, Kushnir Y (2010) Adjustment of the atmospheric circulation to tropical Pacific SST anomalies: variability of transient eddy propagation in the Pacific-North America sector. *Q J R Meteorol Soc* 136:277–296. <https://doi.org/10.1002/qj.588>
- Small RJ, Bryan FO, Bishop SP, Tomas RA (2019) air–sea turbulent heat fluxes in climate models and observational analyses: what drives their variability? *J Clim* 32:2397–2421. <https://doi.org/10.1175/JCLI-D-18-0576.1>
- Small RJ et al (2008) Air–sea interaction over ocean fronts and eddies. *Dyn Atmos Oceans* 45:274–319. <https://doi.org/10.1016/j.dynatmoce.2008.01.001>
- Straus DM, Shukla J (1997) Variations of midlatitude transient dynamics associated with ENSO. *J Atmos Sci* 54:777–790. [https://doi.org/10.1175/1520-0469\(1997\)054<0777:VOMTDA>2.0.CO;2](https://doi.org/10.1175/1520-0469(1997)054<0777:VOMTDA>2.0.CO;2)
- Taguchi B, Nakamura H, Nonaka M, Xie S-P (2009) Influences of the Kuroshio/Oyashio extensions on air–sea heat exchanges and storm-track activity as revealed in regional atmospheric model simulations for the 2003/04 cold season. *J Clim* 22:6536–6560. <https://doi.org/10.1175/2009JCLI2910.1>
- Takatama K, Minobe S, Inatsu M, Small RJ (2012) Diagnostics for near-surface wind convergence/divergence response to the Gulf Stream in a regional atmospheric model. *Atmos Sci Lett* 13:16–21. <https://doi.org/10.1002/asl.355>
- Tokenaga H, Tanimoto Y, Xie SP, Sampe T, Tomita H, Ichikawa H (2009) Ocean frontal effects on the vertical development of clouds over the western North Pacific: in situ and satellite observations. *J Clim* 22:4241–4260. <https://doi.org/10.1175/2009JCLI2763.1>
- Trenberth KE (1991) Storm tracks in the Southern hemisphere. *J Atmos Sci* 48:2159–2178. [https://doi.org/10.1175/1520-0469\(1991\)048<2159:STTSH>2.0.CO;2](https://doi.org/10.1175/1520-0469(1991)048<2159:STTSH>2.0.CO;2)
- Wallace JM, Mitchell TP, Deser C (1989) The influence of sea-surface temperature on surface wind in the eastern equatorial Pacific: seasonal and interannual variability. *J Clim* 2:1492–1499. [https://doi.org/10.1175/1520-0442\(1989\)002<1492:TIOSSH>2.0.CO;2](https://doi.org/10.1175/1520-0442(1989)002<1492:TIOSSH>2.0.CO;2)
- Yao Y, Zhong Z, Yang XQ (2018) Impacts of the subarctic frontal zone on the North Pacific storm track in the cold season: an observational study. *Inter J Climatol* 38:2554–3256. <https://doi.org/10.1002/joc.5429>
- Yao Y, Zhong Z, Yang XQ, Wei L (2017) An observational study of the North Pacific storm-track impact on the midlatitude

oceanic front. *J Geophys Res Atmos* 122:6962–6975. <https://doi.org/10.1002/2016JD026192>

Zhang C, Liu H, Li C, Lin P (2019) Impacts of Mesoscale Sea surface temperature anomalies on the meridional shift of North Pacific storm track. *Int J Climatol* 39:5124–5139. <https://doi.org/10.1002/joc.6130>

Zhang Y, Held IM (1999) A linear stochastic model of a GCM's mid-latitude storm tracks. *J Atmos Sci* 56:3416–3435. [https://doi.org/10.1175/1520-0469\(1999\)056<3416:ALSMOA>2.0.CO;2](https://doi.org/10.1175/1520-0469(1999)056<3416:ALSMOA>2.0.CO;2)

**Publisher's Note** Springer Nature remains neutral with regard to jurisdictional claims in published maps and institutional affiliations.